

Quantum effects in a double-walled carbon nanotube capacitor

Kazuyuki Uchida, Susumu Okada, Kenji Shiraishi, and Atsushi Oshiyama

*Center for Computational Sciences and Institute of Physics, University of Tsukuba, 1-1-1 Tennodai, Tsukuba 305-8577, Japan
and CREST, Japan Science and Technology Agency, 4-1-8 Honcho, Kawaguchi, Saitama 332-0012, Japan*

(Received 9 April 2007; published 30 October 2007)

We have theoretically investigated the capacitance of a double-walled carbon nanotube (CNT) (4,0)@(24,0) as a nanoscale coaxial-cylindrical capacitor. To calculate the responses of the capacitor to the bias application, we have used a first-principles method based on the density-functional theory with a local-density approximation. We show that the capacitance exhibits two principal quantum effects: First, the capacitance shows a large bias dependence, reflecting the density of states of the CNT electrodes. Second, the capacitance is enhanced according to a quantum-mechanical spill of the stored electron density from the tube walls of the CNTs. We argue that these two quantum effects are fundamental factors in nanoscale capacitors.

DOI: [10.1103/PhysRevB.76.155436](https://doi.org/10.1103/PhysRevB.76.155436)

PACS number(s): 73.90.+f, 73.22.Dj, 77.90.+k

I. INTRODUCTION

Capacitance C is a fundamental quantity in electric circuits: It is defined as a ratio of the electric charge Q stored in the electrodes to the applied bias voltage μ , and describes the performances of capacitors ubiquitous in electric circuits. Such an important role of the capacitance has been recognized for a long time and is becoming more prominent in current electron devices, where a variety of capacitors are fabricated in complicated and miniaturized built-in structures. Gate capacitors made of gate stacks, i.e., gate electrodes, insulating films, and channel regions, in field-effect transistors (FETs) are examples, and control of the capacitance is crucial in the design of large-scale integrated circuits.

In current electron devices, the thickness of the gate stack reaches an order of nanometer. In addition, other nanometer structures, such as multigate structures called fin-FET¹ or coaxial-cylindrical gate-channel structures called surrounding gate transistors (SGTs),² are regarded as boosters of future semiconductor technology.

In nanometer-scale structures, capacitance is different from what is expected from the classical electromagnetism. This is because the charge is accommodated in electron states where wave functions have inhomogeneous distributions with the scale of nanometer. In addition, peculiar structures with the nanometer scale, such as surrounding gate structures, may render the characteristics of the dimensionality in electronic structures prominent and hereby affects the capacitance of the nanostructures. The purpose of the present paper is to clarify such quantum effects in nanoscale capacitors that have been rarely addressed in the past.

In order to demonstrate the quantum effects in the capacitance of nanostructures, we here consider double-walled carbon nanotubes (DWCNTs).^{3,4} Carbon nanotube (CNT)⁵ is a fascinating material that shows a metallic or a semiconducting behavior, depending on its radius and chirality.^{6–9} Magnetic ordering related to peculiar edge states^{10–12} is also predicted^{13–15} based on the density-functional theory (DFT).^{16,17} Owing to its robustness in atomic structures and its capability of carrying more currents than conventional semiconductors, CNT is also a candidate material for chan-

nels or gates in future electronics.¹⁸ Double-walled carbon nanotubes may thus be ultimate elements of SGTs and, more scientifically, offer stages where quantum effects in nanometer-scale structures on the capacitance are examined.

In this paper, we present first-principles calculations of capacitance performed for (4,0)@(24,0) DWCNT, in which a (4,0) zigzag CNT is encapsulated in a (24,0) zigzag CNT. The calculations are based on the DFT with a local density approximation (LDA).^{19,20} We have found two principal quantum effects. First, the capacitance shows rich and occasionally spiky structures as a function of the bias voltage. This is due to the Fermi-level increase and decrease in the outer and inner CNTs accompanied by charge accumulations, reflecting characteristics of the density of states (DOS) of the quasi-one-dimensional CNT electrodes. Second, the calculated capacitance is substantially larger than what is expected from the classical electromagnetism with an assumption that the stored charge is distributed on the walls of CNTs. This capacitance enhancement is due to a quantum spill of the stored electron density which thereby reduces the effective separation of the two CNTs. These two features become prominent only in small-size structures and are peculiar to nanoscale capacitors.

The organization of the present paper is as follows. In Sec. II, we explain the geometrical configuration of the DWCNT capacitor. We then explain our methodology in Sec. III. The obtained results are presented in Sec. IV. Section V summarizes our findings.

II. MODEL

Figure 1 shows the DWCNT capacitor investigated in the present paper. The inner is a (4,0) CNT, the minimum zigzag tube that has ever been observed experimentally,²¹ and the outer one is a (24,0) zigzag CNT. The radii of these two CNTs, R_{in} and R_{out} , are 1.7 and 9.4 Å, respectively. The separation of the walls of the two CNTs is thus 7.7 Å, which assures a negligible overlap of electron densities distributed in the two CNTs, hereby constituting a nano scale capacitor.

The (4,0) and (24,0) CNTs are semiconducting and metallic, respectively, when we apply a simple theory in which electron states are determined by putting a circular boundary

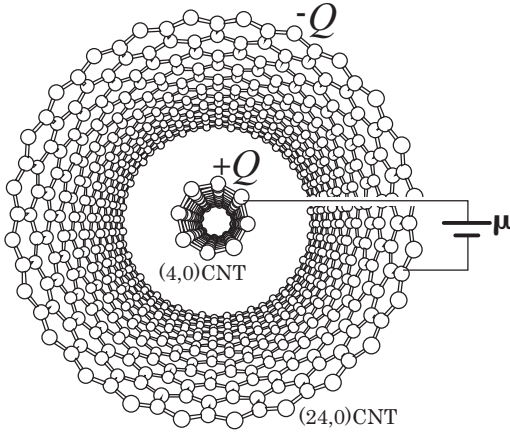


FIG. 1. Double-walled carbon-nanotube capacitor consisting of an inner (4,0) nanotube and an outer (24,0) nanotube. One of the tubes is biased with μ relative to the other, and $\pm Q$ charges are stored. The unit cell is composed of 112 carbon atoms, which is a sum of the 96 outer-tube atoms and 16 inner-tube atoms.

condition to the wave functions in a single graphite sheet. Yet the sp^3 hybridization caused by the finite curvature makes the isolated (4,0) CNT metallic²² and (24,0) semiconducting with a very narrow band gap.⁶ In the DWCNT (4,0)@(24,0) without bias voltage ($\mu=0$), electron transfers from the (24,0) CNT to the (4,0) CNT to some extent so that the Fermi levels of the both CNTs coincide ($\varepsilon_F^{\text{out}} = \varepsilon_F^{\text{in}}$). Then, these CNT electrodes become metallic in the ground state of the capacitor.²³ In this paper, the amount of the stored charge Q under a finite bias voltage μ is measured with reference to this electron distribution in the ground state of the capacitor.

Experimentally, a controlled fabrication of DWCNT capacitors has not been achieved yet. However, a current-induced oxidation technique may be a candidate process.²⁴ Current flow through multiwalled carbon nanotubes (MWCNTs) induces oxidation of outer tubes one by one; then, coaxial-cylindrical CNT shells in which the inner shell is stuck out from the outer shell have been obtained. Two electrodes can be attached to the inner- and outer-CNT shells, respectively. The DWCNT capacitor structure that we discuss in this paper is a representative of such MWCNT capacitors being explored in the experiments.

When investigating the responses of the capacitor to the bias application μ , we perform electron-state calculations of the capacitor in which the Fermi levels of the inner CNT $\varepsilon_F^{\text{in}}$ and the outer CNT $\varepsilon_F^{\text{out}}$ are forced to satisfy the relation of $\varepsilon_F^{\text{out}} = \varepsilon_F^{\text{in}} + \mu$. Details of our scheme is explained in Sec. III. When $\mu > 0$, the outer and inner CNTs are charged negatively ($-Q < 0$) and positively ($+Q > 0$), respectively. Total charge neutrality of the capacitor is preserved in our scheme, though each CNT electrode is charged by $\pm Q$. According to the calculated $Q-\mu$ relation, we obtain the capacitance $C (= \frac{dQ}{d\mu})$ of the DWCNT capacitor.

In practical calculations, we use a supercell model in which an infinite-length DWCNT capacitor is placed in a cell with enough vacuum region, and each cell is arranged in a tetragonal lattice with the lattice constants of $a=27 \text{ \AA}$ and $c=4.3 \text{ \AA}$. The lattice constant c corresponds to the common

periodicity of the (4,0) and (24,0) CNTs along the tube direction. In the directions perpendicular to the tubes, on the other hand, each DWCNT is separated by at least 8.2 \AA from adjacent DWCNTs. This separation of the capacitors ensures that electron distribution is confined within each capacitor. Also, electrostatic field exists only between the two electrodes in each capacitor. Interactions among the capacitor and its mirrors are thus safely negligible. Hence, our supercell model describes a single DWCNT capacitor isolated in vacuum. The unit cell contains 112 carbon atoms, which are the sum of the 16 inner-tube atoms and the 96 outer-tube atoms.

III. METHOD

The capacitance is calculated from the electron redistribution in the capacitor under the bias voltage μ , where the Fermi levels of the inner CNT $\varepsilon_F^{\text{in}}$ and the outer CNT $\varepsilon_F^{\text{out}}$ satisfy the relation of $\varepsilon_F^{\text{out}} = \varepsilon_F^{\text{in}} + \mu$. We first calculate the electron distribution $\rho_0(\mathbf{r})$ in the ground state of the capacitor by using a usual DFT-LDA electron-state calculation^{16,17,19,20} with pseudopotentials^{25,26} under a zero bias voltage ($\mu=0$). We next define the electron redistribution $\Delta\rho_\mu(\mathbf{r})$ induced by the bias application as

$$\Delta\rho_\mu(\mathbf{r}) = \rho_\mu(\mathbf{r}) - \rho_0(\mathbf{r}), \quad (1)$$

where $\rho_\mu(\mathbf{r})$ is the electron distribution under the bias voltage μ . The total number N^{all} of the electrons in the capacitor is preserved regardless of the bias voltage μ in our scheme and is calculated as

$$N^{\text{all}} = \int \rho_0(\mathbf{r}) d\mathbf{r} = \int \rho_\mu(\mathbf{r}) d\mathbf{r}. \quad (2)$$

This assures the total charge neutrality of the system even after the bias application.

By using $\Delta\rho_\mu(\mathbf{r})$, the quantity of excess electrons ΔN stored in the outer CNT is calculated as

$$\Delta N[\rho_\mu(\mathbf{r})] = \int \Delta\rho_\mu(\mathbf{r}) \Theta(\mathbf{r}) d\mathbf{r}, \quad (3)$$

where $\Theta(\mathbf{r})$ is defined as

$$\Theta(\mathbf{r}) = \begin{cases} 0 & \text{for } \mathbf{r} \in \text{the inner-CNT region} \\ 1 & \text{for } \mathbf{r} \in \text{the outer-CNT region.} \end{cases} \quad (4)$$

In Eq. (4), we have divided the system into two parts, the inner-tube region and the outer-tube region. The boundary between the two regions is placed in the vacuum between the inner and outer tubes, where the electron density sufficiently diminishes. As shown below, the density at the boundary is smaller by an order of 10^{-5} than the density near tube walls in the present DWCNT. The same quantity ΔN of electrons is depleted in the inner CNT, as the total number N^{all} of the electrons in the capacitor is preserved in our calculations. Then, the stored charge Q in the DWCNT capacitor is defined as $Q = e\Delta N[\rho_\mu(\mathbf{r})]$. In the present paper, we restrict ourselves to the case that the electron density at the boundary region is small enough so that the leakage current between two CNTs is negligible.

We subsequently define an energy Ω (Ref. 27–29) by using $\Delta N[\rho_\mu(\mathbf{r})]$ as

$$\Omega[\rho_\mu(\mathbf{r})] = E[\rho_\mu(\mathbf{r})] - \mu \Delta N[\rho_\mu(\mathbf{r})]. \quad (5)$$

This is a functional of the electron density $\rho_\mu(\mathbf{r})$ under a fixed bias voltage μ : The first term E of Eq. (5) is the total energy of the capacitor, described by the DFT-LDA scheme with the pseudopotentials. The second term, $-\mu \Delta N$, describes a situation where the power source with the bias voltage μ is attached to the capacitor.

By minimizing Ω with respect to $\rho_\mu(\mathbf{r})$, we obtain the electron distribution under the bias voltage μ .³⁰ In a practical procedure of the minimization, the electron density $\rho_\mu(\mathbf{r})$ is expressed in terms of one-electron orbitals $\phi_n(\mathbf{r})$ as

$$\rho_\mu(\mathbf{r}) = \sum_{\varepsilon_n \leq \varepsilon_F}^{N^{\text{all}}} |\phi_n(\mathbf{r})|^2, \quad (6)$$

where the energy ε_F is determined so that the total number of electrons amounts to N^{all} , as described in Eq. (2). The relation between the upper-limit energy ε_F and the Fermi levels of the inner and outer CNTs, $\varepsilon_F^{\text{in}}$ and $\varepsilon_F^{\text{out}}$, is explained later. Substituting Eq. (6) into Eq. (5), and solving the variational problem of Ω with respect to $\phi_n(\mathbf{r})$ analytically, we obtain a modified Kohn-Sham equation,

$$[\hat{H}_{\text{KS}} - \mu \Theta(\mathbf{r})] \phi_n(\mathbf{r}) = \varepsilon_n \phi_n(\mathbf{r}). \quad (7)$$

Here, \hat{H}_{KS} is a usual Kohn-Sham Hamiltonian originated from the first term E of Eq. (5). \hat{H}_{KS} depends on $\rho_\mu(\mathbf{r})$ and is a sum of the kinetic-energy operator, the ionic pseudopotentials describing nuclei and core electrons, the Hartree potential, and the exchange-correlation potential among valence electrons. The term $-\mu \Theta(\mathbf{r})$ is an additional effective potential derived from the second term of Eq. (5). By solving Eqs. (6) and (7) self-consistently, we obtain the electron distribution $\rho_\mu(\mathbf{r})$ and redistribution $\Delta \rho_\mu(\mathbf{r})$, and then the quantity of the stored charge $Q (= e \Delta N[\rho_\mu(\mathbf{r})])$ in the capacitor as a function of the bias voltage μ . The Q - μ relation of the capacitor is obtained in this way. We then calculate the differential capacitance C , defined as

$$C = \frac{dQ}{d\mu}. \quad (8)$$

We here explain the interpretation of the eigenvalue ε_n obtained from Eq. (7). When $\phi_n(\mathbf{r})$ is an eigenstate, we obtain

$$\varepsilon_n = \langle \phi_n | \hat{H}_{\text{KS}} | \phi_n \rangle - \mu \langle \phi_n | \Theta(\mathbf{r}) | \phi_n \rangle. \quad (9)$$

The first term of Eq. (9) is the one-electron energy in a natural meaning, whereas its second term is an extra one due to the contact of the power source. In discussing the one-electron energy spectrum, we thus exclude the contributions of the second term from the calculated ε_n values.

We can classify the one-electron states $\{\phi_n\}$ into inner-tube states $\{\phi_n^{\text{in}}\}$ and outer-tube states $\{\phi_n^{\text{out}}\}$.³¹ As $\langle \phi_n^{\text{in}} | \Theta(\mathbf{r}) | \phi_n^{\text{in}} \rangle = 0$, we regard ε_n of the inner-tube state as its one-electron energy. We correct the one-electron energy of

the outer-tube state as $\varepsilon_n \rightarrow \varepsilon_n + \mu$ because of the relation of $\langle \phi_n^{\text{out}} | \Theta(\mathbf{r}) | \phi_n^{\text{out}} \rangle = 1$. According to this procedure, the Fermi level of the outer CNT $\varepsilon_F^{\text{out}}$ is corrected as $\varepsilon_F + \mu$, whereas that of the inner CNT $\varepsilon_F^{\text{in}}$ remains to be ε_F in Eq. (6), naturally satisfying the condition of $\varepsilon_F^{\text{out}} = \varepsilon_F^{\text{in}} + \mu$.

In the present calculations, nuclei and core electrons are simulated by ultrasoft pseudopotentials (USPPs),²⁶ which enable us to calculate electron states with sufficient accuracy and at reasonable computing costs. When using the USPPs, Eqs. (6) and (7) are slightly generalized according to the treatment in Ref. 26 to compensate for the deficit in the electron charge in this pseudopotential formalism. We take the core radius $r_c = 1.2$ a.u. for $2s$ and $2p$ orbitals. Interactions among valence electrons are treated by the local-density approximation.^{19,20} The modified Kohn-Sham equation [Eq. (7)] is solved by using a conjugate-gradient (CG) minimization technique. Ionic configurations are also optimized by the CG minimization. We have indeed performed the structural optimization of the DWCNT at $\mu = 0$, under a restriction that the two CNTs are in the coaxial configuration. All the computations have been performed by using the TAPP code.³²

There are several other approaches to the capacitance from first principles: For example, nonequilibrium Green's-function formalism³³ and a wave-function matching method³⁴ combined with the DFT have already been proposed. Computational costs of these approaches in the past are higher than usual DFT calculations for ground states. In contrast, our scheme is formulated by the minimization of the energy Ω in Eq. (5), and the modified Kohn-Sham equation [Eq. (7)] is the same as that in the ground-state calculations except for the additional effective potential, $-\mu \Theta(\mathbf{r})$. This infers that the computational cost of our methodology is almost comparable with that for the ground states.

Helped by such a reasonable computing cost of our scheme, we have performed highly accurate Brillouin-zone integrations with 50 k -point samplings along the tube direction. We have employed a plane-wave basis set to expand the one-electron wave function $\phi_n(r)$ with the cutoff energy chosen as 36 Ry. As will be discussed in Sec. IV, singularities in the density of states and deformations of the wave functions affect the capacitance substantially. Hence, the precise Brillouin-zone integrations and the completeness of the basis set are essential to obtain accurate capacitance.

IV. RESULTS AND DISCUSSIONS

A. Electron redistribution and potential variation

We first demonstrate how the applied bias μ induces redistribution $\Delta \rho_\mu(r)$ of the electron density and then the potential variation $\Delta V_\mu(r)$ in the DWCNT structure. Figures 2(a) and 2(b) shows the calculated $\Delta \rho_\mu(\mathbf{r})$ at the bias voltage $\mu = 2.7$ eV. The outer (24,0) CNT is negatively charged, whereas the inner (4,0) CNT is positively charged. Here, the inner- and outer-CNT regions are separated at a radius of 5.6 Å, and the redistribution $\Delta \rho_\mu(r)$ at this radius is at most $\sim 2.5 \times 10^{-5} e/\text{Å}^3$, being diminished sufficiently. As the electron density $\rho_\mu(r)$ at this radius is smaller than the densities

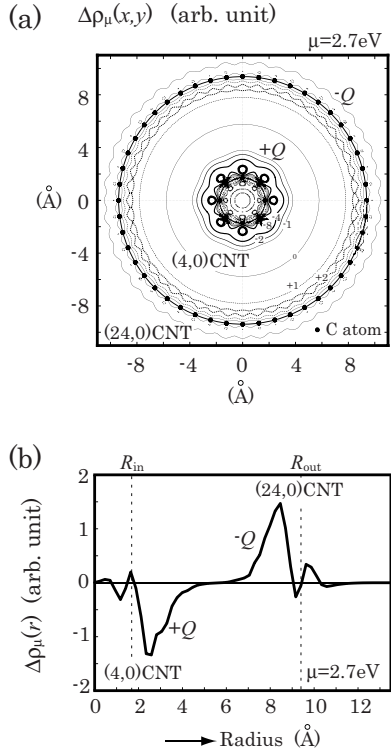


FIG. 2. Redistribution $\Delta\rho_\mu(\mathbf{r})$ of the electron density induced by the bias voltage $\mu=2.7$ eV. Stored charge is calculated to be $Q=0.33 e/\text{unit cell}$. (a) Contour plots of $\Delta\rho_\mu$ projected on a cross section perpendicular to the tube axis: $\Delta\rho_\mu(x,y)\equiv\int\Delta\rho_\mu(\mathbf{r})dz$. (b) Profile of $\Delta\rho_\mu$ along the radial coordinate r : $\Delta\rho_\mu(r)\equiv\int\Delta\rho_\mu(\mathbf{r})dzd\theta$.

near CNT walls, $\sim 2 e/\text{\AA}^3$, by an order of 10^{-5} , we can neglect current leakage between the CNTs in the present case. The accumulated charge Q is calculated to be $0.33 e/\text{unit cell}$.

The projected $\Delta\rho_\mu(\mathbf{r})$ on the cross section of the CNTs [Fig. 2(a)] and on the radial direction [Fig. 2(b)] clearly shows characteristic features of the redistribution. Accumulated charge distribution is correlated with the arrangements of the carbon atoms as in Fig. 2(a), indicating that the stored

charge is accommodated in the carbon π orbitals. An interesting aspect is that the accumulated charge is spilled from the tube wall of the CNTs. Excess electrons of the outer CNT penetrates inside, whereas the depleted region of the inner tube extends outside, as shown in Fig. 2(b).

The redistribution of the electron density $\Delta\rho_\mu(\mathbf{r})$ also induces the potential variation $\Delta V_\mu(\mathbf{r})$ defined as

$$\Delta V_\mu(\mathbf{r}) = V_\mu(\mathbf{r}) - V_0(\mathbf{r}), \quad (10)$$

where $V_\mu(\mathbf{r})$ and $V_0(\mathbf{r})$ are the sums of the Hartree potential, the exchange-correlation potential, and the electrostatic potential from ions in terms of the pseudopotentials, and are calculated with and without the bias application, respectively. Figure 3(c) shows the calculated $\Delta V_\mu(\mathbf{r})$ at the bias voltage $\mu=2.7$ eV. Between the inner and outer tubes, there exists a potential difference V defined as

$$V = V_{\text{out}} - V_{\text{in}}, \quad (11)$$

where $V_{\text{in}}[\equiv\Delta V_\mu(R_{\text{in}})]$ and $V_{\text{out}}[\equiv\Delta V_\mu(R_{\text{out}})]$ are, by our definition, the potential levels of the inner and outer tubes, respectively. We have found that V is almost explained by the contribution from the Hartree potential. Thus, we can regard V as the electrostatic potential shift induced by the electric charging of the outer CNT ($-Q$) and the inner CNT ($+Q$). We have also found that the obtained potential shift V is definitely smaller than the applied bias voltage μ . This discrepancy is discussed in detail in the next subsection.

B. Capacitance

Figure 4(a) shows the calculated capacitance C defined as Eq. (8). From this figure, we find two principal quantum effects. First, C strongly depends on the bias μ , which is in contrast with the *bias-independent* capacitance in the classical electromagnetism. Second, C is larger than the classical expectation C_{cla} , which is defined as

$$C_{\text{cla}} = \frac{2\pi\epsilon_0}{\ln(R_{\text{out}}/R_{\text{in}})} \sim 3.4 \times 10^{-21} \text{ F/\AA}, \quad (12)$$

from the electromagnetism with an assumption that the stored charge is distributed on the tube walls of the CNTs.

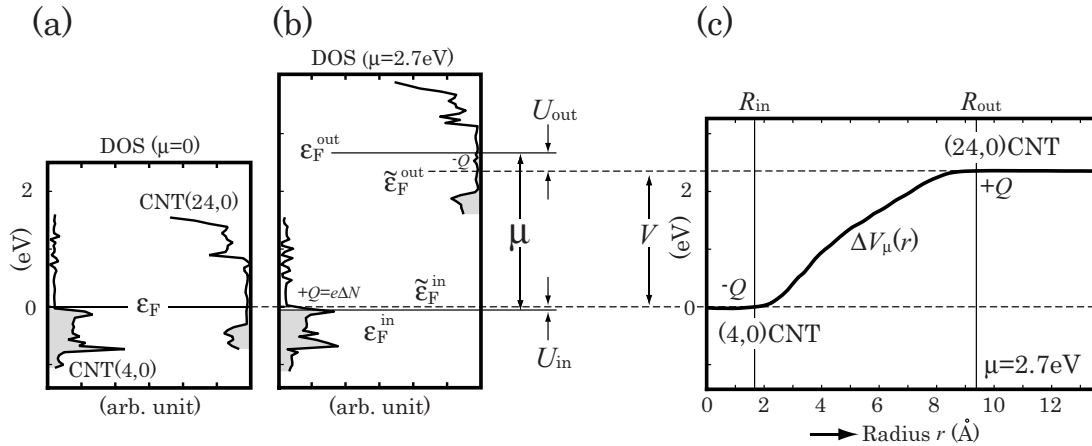


FIG. 3. [(a)–(b)] DOS of the inner (4,0) CNT and outer (24,0) CNT under the bias voltage (a) $\mu=0$ eV and (b) $\mu=2.7$ eV. (c) Variation $\Delta V_\mu(\mathbf{r})$ in the potential along the radial coordinate, induced by the bias voltage $\mu=2.7$ eV: $\Delta V_\mu(r)=\int\Delta\rho_\mu(\mathbf{r})dzd\theta/\int dzd\theta$.

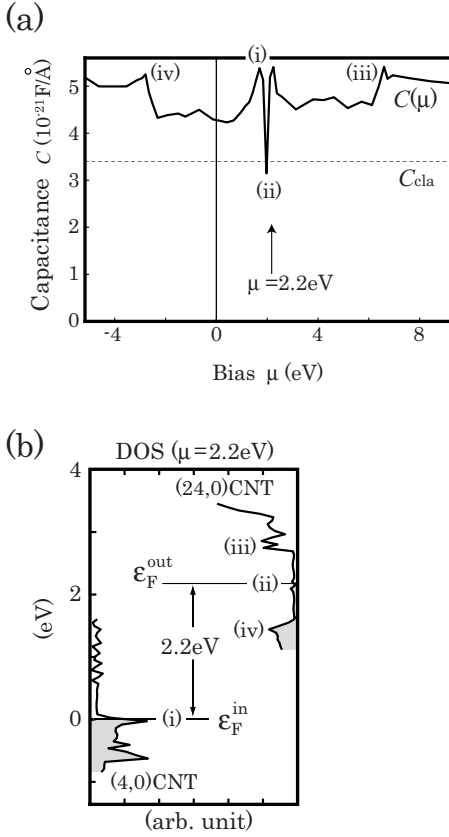


FIG. 4. (a) Bias dependence of the capacitance $C(\mu)$. (b) DOS of the inner (4,0) CNT and outer (24,0) CNT under the bias voltage $\mu=2.2$ eV.

In the following, we clarify the origins of these two quantum effects in the capacitance: We show that the former effect is a reflection of the DOS structures of the CNTs and that the latter is due to the spill of the stored electron density from the tube walls of the CNTs. We also perform a detailed analysis of the electron redistribution $\Delta\rho_\mu(\mathbf{r})$ in terms of the electron states of the capacitor, which provides us with a deeper understanding of the capacitance in nanoscale systems.

1. Bias-voltage dependence of capacitance

First, we show that the former quantum effect, the bias dependence of the capacitance $C(\mu)$, originates from the DOS structures of the CNT electrodes. For an explanation of this point, we show in Figs. 3(a) and 3(b) the DOS of the inner (4,0) and outer (24,0) CNTs under the bias voltage (a) $\mu=0$ eV and (b) $\mu=2.7$ eV. We observe characteristic spiky peaks, which are Van Hove singularities reflecting the quasi-one-dimensionality of the CNTs. We find that these DOS structures of the inner and outer CNTs are almost rigid except for their relative shift after the bias application. As we already mentioned, the Fermi level of the outer CNT $\varepsilon_F^{\text{out}}$ is higher than that of the inner CNT $\varepsilon_F^{\text{in}}$ by the applied bias voltage μ , $\varepsilon_F^{\text{out}} = \varepsilon_F^{\text{in}} + \mu$.

In Fig. 3(b), the excess $\Delta N (= Q/e)$ electrons are stored in the outer (24,0) CNT, filling the electron states in the energy range of $\tilde{\varepsilon}_F^{\text{out}} \leq \varepsilon \leq \varepsilon_F^{\text{out}}$. The electron state at $\tilde{\varepsilon}_F^{\text{out}}$ in Fig. 3(b)

corresponds to that at ε_F in Fig. 3(a). As for the inner (4,0) CNT, on the other hand, the electron states in the energy range of $\varepsilon_F^{\text{in}} \leq \varepsilon \leq \tilde{\varepsilon}_F^{\text{in}}$ are empty in (b), which explains the depletion of ΔN electrons out of the inner CNT.

The relative shift of the DOS between the inner and outer CNTs induced by the bias application is quantified by $\tilde{\varepsilon}_F^{\text{out}} - \tilde{\varepsilon}_F^{\text{in}}$. We find that this quantity coincides with the electrostatic potential shift V calculated by Eq. (11), $\tilde{\varepsilon}_F^{\text{out}} - \tilde{\varepsilon}_F^{\text{in}} \sim V$, as shown in Figs. 3(b) and 3(c). This means that the shift of the DOS after the bias application is brought about by that of the electrostatic potential. We decompose the bias voltage μ as

$$\begin{aligned} \mu &\equiv \varepsilon_F^{\text{out}} - \varepsilon_F^{\text{in}} = (\varepsilon_F^{\text{out}} - \tilde{\varepsilon}_F^{\text{out}}) + (\tilde{\varepsilon}_F^{\text{out}} - \tilde{\varepsilon}_F^{\text{in}}) + (\tilde{\varepsilon}_F^{\text{in}} - \varepsilon_F^{\text{in}}) \\ &= U^{\text{out}} + V + U^{\text{in}}. \end{aligned} \quad (13)$$

Here, $U^{\text{out}} (\equiv \varepsilon_F^{\text{out}} - \tilde{\varepsilon}_F^{\text{out}})$ and $U^{\text{in}} (\equiv \tilde{\varepsilon}_F^{\text{in}} - \varepsilon_F^{\text{in}})$ are the Fermi-level shifts that originate from the Fermi statistics of electrons: When finite-value DOS is newly occupied (emptied) by electrons, the Fermi-energy levels shift upward (downward) within the DOS of each CNT electrode. In macroscopic capacitors, V is much larger than U^{in} and U^{out} , and thus we can almost equate μ with V . In nanoscale systems such as the present DWCNT capacitor, however, we are unable to neglect the contributions from U^{in} and U^{out} to the bias voltage μ , as shown in Figs. 3(b) and 3(c), which significantly influence the capacitance as explained below.

Substituting Eq. (13) into Eq. (8), we obtain the following expression of the capacitance $C(\mu)$:

$$\begin{aligned} C(\mu)^{-1} &\equiv d\mu/dQ = dV/dQ + dU^{\text{in}}/dQ + dU^{\text{out}}/dQ \\ &= C_0^{-1} + D_{\text{in}}^{-1} + D_{\text{out}}^{-1}. \end{aligned} \quad (14)$$

This means that the inverse of the total capacitance C is a sum of the inverses of the electrostatic capacitance $C_0 (\equiv dQ/dV)$, the inner-tube DOS $D_{\text{in}} (\equiv dQ/dU^{\text{in}})$ at the Fermi level $\varepsilon_F^{\text{in}}$, and the outer-tube DOS $D_{\text{out}} (\equiv dQ/dU^{\text{out}})$ at $\varepsilon_F^{\text{out}}$. We recognize that $0 \leq C \leq C_0$, and $C \rightarrow C_0$ when D_{in} and D_{out} are large enough, whereas $C \rightarrow 0$ when D_{in} or D_{out} is small enough.

The calculated electrostatic capacitance C_0 is $\sim 5.4 \times 10^{-21}$ F/Å, which is in good agreement with the maximal value of $C(\mu)$ observed in Fig. 4(a). We have found that the bias dependence of C_0 is small, and we thus expect that the bias dependence of $C(\mu)$ almost originates from the contributions of the DOS terms, D_{in} and D_{out} . Such a contribution of the DOS to the capacitance was first theoretically pointed out by Büttiker³⁵ in mesoscopic systems and had been confirmed in experiments in semiconductor quantum dots.³⁶ As demonstrated below, the DWCNT capacitor is a good example to demonstrate this effect in nanoscale materials because of its characteristic spiky DOS structures peculiar to quasi-one-dimensional systems.

We have confirmed that the obtained structure of $C(\mu)$ corresponds to those of $D_{\text{in}}(\varepsilon)$ and $D_{\text{out}}(\varepsilon)$: The singular points of $C(\mu)$ [(i)–(iv) in Fig. 4(a)] appear just when the Fermi levels $\varepsilon_F^{\text{in}}$ and $\varepsilon_F^{\text{out}}$ cross the singular points in the DOS of the inner and outer tubes [(i)–(iv) in Fig. 4(b)]. In Fig. 4(b), (i), (iii), and (iv) are Van Hove singularities peculiar to quasi-one-dimensional systems, while (ii) is a V-like dip, i.e.,

a very small band gap, between the conduction-band bottom and the valence-band top of the (24,0) CNT. The plateau regions in $C(\mu)$ also correspond to those in D_{in} and D_{out} , and the magnitude of C is correlated with those of D_{in} and D_{out} .

For example, when $\mu=2.2$ eV, the Fermi levels $\varepsilon_F^{\text{in}}$ and $\varepsilon_F^{\text{out}}$ are just on the singular points of the DOS indicated by (i) and (ii) in Fig. 4(b), respectively. The singular behaviors of $C(\mu)$ observed at (i) and (ii) in Fig. 4(a) are their reflections. In this way, we understand that the large bias dependence of the capacitance originates from the DOS structures of the CNTs. An accurate calculation of the DOS is essential to demonstrate this effect. The reflections of the Van Hove singularities in the DOS to the capacitance were not demonstrated in a previous DFT calculation in DWCNT capacitors.³³ We have sampled 50 k points along the tube axis in Brillouin-zone integrations in this study and have succeeded in showing the correspondence between the DOS of the CNTs, D_{in} and D_{out} , and the capacitance $C(\mu)$ clearly. Recent experimental works^{37,38} on CNT-based FETs infer that the DOS structure of the CNTs affects the capacitance of the FET structures. This may be a demonstration of our findings, although the data contain some ambiguities.

Experimentally, CNTs have finite lengths. When its aspect ratio, i.e., the ratio of its length to its diameter, is high, the finite-length CNT is regarded as an infinite-length system. In the case, the Van Hove singularity of the one-dimensional system is prominent in DOS and then in its capacitance. When the aspect ratio becomes low, the Van Hove singularity related to the one dimensionality becomes less prominent. Discreteness of the level structure, which is peculiar to a zero-dimensional system, may play an important role in the capacitance in the case.

We comment that DOS structures of nanomaterials are, in general, not always rigid in response to the bias application. For example, the atomic structures of materials with electric-dipole moments can be substantially deformed²⁷ under the bias voltage, modulating their DOS structures. Also, the DOS of the systems with latent magnetic instability³⁹ can be strongly deformed when ferro- or antiferromagnetism is induced by the bias application. In this sense, materials with drastic changes in the atomic and electronic structures when electrically charged^{40–43} are promising substances to fabricate nanoscale capacitors showing novel responses to the bias applications.

2. Enhancement of capacitance

Next, we discuss the origin of the latter quantum effect: the enhancement of the calculated capacitance C compared with the classical capacitance C_{cla} defined as in Eq. (12). As realized from Eq. (14), C is composed of the electrostatic capacitance C_0 and the DOS of the inner and outer CNTs, D_{in} and D_{out} . We have found that the first component C_0 is larger than C_{cla} . Also, the second and third components $D_{\text{in}}(\geq 0)$ and $D_{\text{out}}(\geq 0)$ make only reductive contributions to C . Therefore, the enhancement of C comes from the enhancement of C_0 .

As expected easily, this enhancement of the electrostatic capacitance C_0 is associated with the spill of the stored electron density from the tube walls with the radii R_{in} and R_{out} .

As discussed in Sec. IV A, the stored electron density in the inner (outer) CNT spills outward (inward) and reduces the effective electrode-electrode separation and thus enhances the electrostatic capacitance.

To show this point clearly, we here introduce spill lengths Δ_{in} and Δ_{out} , and effective radii $R_{\text{in}}^{\text{eff}}(\equiv R_{\text{in}} + \Delta_{\text{in}})$ and $R_{\text{out}}^{\text{eff}}(\equiv R_{\text{out}} - \Delta_{\text{out}})$ in the inner and outer CNTs. From Fig. 2(b), it is natural that $R_{\text{in}}^{\text{eff}}$ ($R_{\text{out}}^{\text{eff}}$) is chosen at the center of mass of the outermost (innermost) spilled part of $\Delta\rho_{\mu}(r)$ in the inner (outer) CNT. Then, the spill lengths of the stored charge from the tube walls are estimated to be $\Delta_{\text{in}} \sim \Delta_{\text{out}} \sim 1 \text{ \AA}$. By using such effective radii $R_{\text{in}}^{\text{eff}}$ and $R_{\text{out}}^{\text{eff}}$, we are able to reproduce the calculated value of the electrostatic capacitance C_0 through the classical electromagnetic formula as

$$\frac{2\pi\epsilon_0}{\ln(R_{\text{out}}^{\text{eff}}/R_{\text{in}}^{\text{eff}})} = \frac{2\pi\epsilon_0}{\ln\{(R_{\text{out}} - \Delta_{\text{out}})/(R_{\text{in}} + \Delta_{\text{in}})\}} \sim C_0 (= 5.4 \times 10^{-21} \text{ F/\AA}). \quad (15)$$

This means that the enhancement of the (electrostatic) capacitance is certainly explained by the spill of the stored charge from the tube walls of the CNTs.

Supplementarily, we here point out an asymmetry between the inner and outer tubes concerned with the enhancement of the electrostatic capacitance C_0 . The spill lengths in the inner and outer tubes are almost the same, $\Delta_{\text{out}} \sim \Delta_{\text{in}}$. However, as is realized from Eq. (15), Δ_{in} more strongly contributes to the enhancement of C_0 than Δ_{out} . This is due to the coaxial-cylindrical geometry of the present capacitor: The surface of the inner electrode is narrower than that of the outer electrode. Due to the higher concentration of the electric flux in the narrower space, the electric field on the inner-tube surface is larger than that on the outer-tube surface. The spill under the larger electric field more strongly reduces the potential shift V between the electrodes and, thus, more strongly enhances the electrostatic capacitance C_0 . This is why Δ_{in} more strongly contributes to the enhancement of C_0 than Δ_{out} .

3. Dielectric responses in $\Delta\rho_{\mu}(\mathbf{r})$

Third, we perform a detailed analysis on the redistribution $\Delta\rho_{\mu}(\mathbf{r})$ of the electron density in terms of the electron states of the capacitor. As we have already mentioned, the electron (hole) just below (above) the Fermi level $\varepsilon_F^{\text{out}}$ ($\varepsilon_F^{\text{in}}$) of the outer (inner) CNT is the newly injected one under the application of the bias voltage $\mu(>0)$. Accommodations of these electrons and holes in the lowest unoccupied (LU) and the highest occupied (HO) states, respectively, lead to the change in the electron density $\Delta\rho_{\mu}^{\text{LH}}(\mathbf{r})$ calculated as

$$\Delta\rho_{\mu}^{\text{LH}}(\mathbf{r}) = \int_{\varepsilon_F^{\text{out}}}^{\varepsilon_F^{\text{in}}} L_{\mu}^{\text{out}}(\mathbf{r}, \varepsilon) d\varepsilon - \int_{\varepsilon_F^{\text{in}}}^{\varepsilon_F^{\text{out}}} L_{\mu}^{\text{in}}(\mathbf{r}, \varepsilon) d\varepsilon, \quad (16)$$

where $L_{\mu}^{\text{in}}(\mathbf{r}, \varepsilon)$ and $L_{\mu}^{\text{out}}(\mathbf{r}, \varepsilon)$ are the local density of states of the inner and outer CNTs, respectively.

Figure 5 shows the calculated $\Delta\rho_{\mu}^{\text{LH}}(\mathbf{r})$ at the bias voltage $\mu=2.7$ eV, which reflects π -orbital characters of the norm of the wave functions of the LU/HO states involved in the

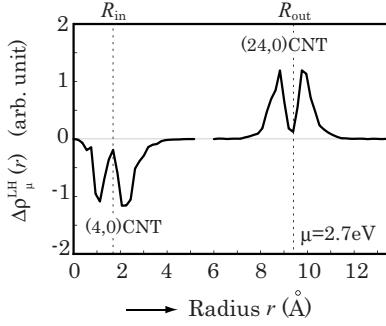


FIG. 5. Change in the electron density $\Delta\rho_{\mu}^{\text{LH}}(\mathbf{r})$ directly caused by the electron/hole accommodation in the LU/HO states of the outer/inner CNT under the bias voltage $\mu=2.7$ eV.

electron/hole accommodations. At a glance, $\Delta\rho_{\mu}^{\text{LH}}(\mathbf{r})$ is similar to $\Delta\rho_{\mu}(\mathbf{r})$ shown in Fig. 2(b). The spill lengths Δ_{in} and Δ_{out} of the stored charge in $\Delta\rho_{\mu}(r)$ are, however, about twice as large as those of the π orbitals observed in $\Delta\rho_{\mu}^{\text{LH}}(r)$. Hence, the spill length and the electrostatic capacitance C_0 are unable to be understood only from the electron/hole accommodation in the LU/HO states. We thus have to consider the other component in $\Delta\rho_{\mu}(\mathbf{r})$, which is labeled as $\Delta\rho_{\mu}^{\text{DE}}(\mathbf{r})$,

$$\Delta\rho_{\mu}(\mathbf{r}) = \Delta\rho_{\mu}^{\text{LH}}(\mathbf{r}) + \Delta\rho_{\mu}^{\text{DE}}(\mathbf{r}). \quad (17)$$

As $\Delta\rho_{\mu}^{\text{DE}}(\mathbf{r})$ is not directly related to the electron/hole accommodation in the LU/HO states, it is naturally attributed to dielectric responses, i.e., deformations of the wave functions, of the electron states which remain fully occupied irrespective of the bias application. We have found that the deformation of each wave function is much smaller than the wave function itself. The total sum of the deformations $\Delta\rho_{\mu}^{\text{DE}}(r)$, however, is large enough to be comparable with $\Delta\rho_{\mu}^{\text{LH}}(r)$. The plane-wave basis set, which we have used in this paper, is suitable for describing such deformations of the wave functions accurately, compared with the linear-combination-of-atomic-orbital basis sets.

We have found that the deformation of the π orbitals is dominant in $\Delta\rho_{\mu}^{\text{DE}}(\mathbf{r})$, compared with that of the σ orbitals. This is explained by the real-space distributions of their wave functions. The tails of the π wave functions are considerably extended toward the vacuum region between the tubes and are exposed to a large electric field to be deformed. On the other hand, the σ orbitals on the tube walls are almost frozen even after the bias application, as the electric field is already screened at the innermost (outermost) tails of the π wave functions in the outer (inner) CNT. The position of the innermost (outermost) tails of the π wave functions in the outer (inner) CNT can be another measure for estimating the effective radius and the spill length in the CNT, which are actually in good agreement with those estimated from the center of mass in $\Delta\rho_{\mu}(\mathbf{r})$, in Sec. IV B 2.

The characters of the one-electron wave functions slightly differ from band to band. The spill lengths Δ_{in} and Δ_{out} of the stored charge hardly vary, however, even when the bias μ is swept and the characters of the bands at the Fermi levels $\varepsilon_F^{\text{in}}$ and $\varepsilon_F^{\text{out}}$ change. This is because the contribution from the dielectric response $\Delta\rho_{\mu}^{\text{DE}}(r)$ is dominant in determining Δ_{in}

and Δ_{out} , and the slight variations in $\Delta\rho_{\mu}^{\text{LH}}(r)$ is obscured. Of course, the spill length may vary substantially when injected electrons or holes are accommodated in the electron states with quite different characters from the π orbitals. For example, such will indeed be the case if the injected electrons are accommodated in nearly free electron (NFE)^{44,45} states of the CNTs, though no NFE state is involved within the calculated bias range in this paper.

The analysis of $\Delta\rho_{\mu}(\mathbf{r})$ also provides us with a deep insight into the field-effect doping in nanoscale systems: Suppose that infinitesimal bias voltage is applied parallel to the tube axes in addition to the tube-tube bias voltage μ . The induced current along these tubes is expected to be carried by the electron states just on the Fermi levels $\varepsilon_F^{\text{in}}$ and $\varepsilon_F^{\text{out}}$. Thus, the carrier distribution is closely related to $\Delta\rho_{\mu}^{\text{LH}}(r)$, not to $\Delta\rho_{\mu}(r)$. This means that the carrier distribution associated with the current flow can be substantially different from the charge distribution explaining the capacitance. This knowledge influences interpretations of experiments when estimating the carrier density and also the design and control of CNT-based FETs and other nanodevices.

C. Role of nanoscale geometries

In closing of the discussion, we consider the reason why the capacitance of the present system shows large quantum effects. As stated above, the quantum effects in the capacitance originate from the spill of the stored charge leading to the electrostatic capacitance C_0 and the contributions from the DOS of the electrodes leading to the total capacitance C .

We first discuss how the effect of charge spill changes with increasing tube radii. We have calculated the spill length in a parallel-plate capacitor of a pair of graphite sheets ($R_{\text{in}}, R_{\text{out}} \rightarrow \infty$). The calculated value is ~ 1 Å, being almost the same as those in the (4,0) and (24,0) CNTs and inferring that the spill length is insensitive to the CNT radii. Hence, when the inner- and outer-electrode radii are large, the ratio of the spill length to the radius is small and thus the effect of charge spill is unimportant. In such a case, from Eqs. (12) and (15), the *electrostatic* capacitance C_0 becomes equal to the classical electromagnetic one, C_{cla} ,

$$C(\mu)^{-1} = C_0^{-1} + D_{\text{in}}^{-1} + D_{\text{out}}^{-1} \sim C_{\text{cla}}^{-1} + D_{\text{in}}^{-1} + D_{\text{out}}^{-1}. \quad (18)$$

We next consider the contributions from D_{in} and D_{out} . When R_{in} and R_{out} become infinite, the DOS of the CNT electrodes approach that of a graphite sheet scaled by the number of the carbon atoms. As the number of atoms is proportional to the radius, the DOS terms scale as $D_{\text{in/out}} \propto R_{\text{in/out}}$. Thus, we expect that

$$C(\mu)^{-1} \sim C_{\text{cla}}^{-1} + D_{\text{in}}^{-1} + D_{\text{out}}^{-1} \sim O[\ln(R_{\text{out}}/R_{\text{in}})] + O(R_{\text{in}}^{-1}) + O(R_{\text{out}}^{-1}). \quad (19)$$

When the tube radii approach infinity with the ratio of the outer- and inner-electrode radii fixed at a constant, the contributions from the DOS will become negligible compared with the electrostatic capacitance. In such cases, we are eventually able to equate the *total* capacitance C with the classical electromagnetic one, C_{cla} . This is a macroscopic

limit where the classical electromagnetism works. In other cases, contributions from the DOS terms can remain finite in the capacitance. For instance, if the tube-tube separation, $R_{\text{out}} - R_{\text{in}}$, is fixed at a small value, we are unable to neglect the contributions from the DOS even when the radii of the inner and outer CNTs approach infinity.

From these analyses, we understand that the large quantum effects in the capacitance observed in the present DWCNT capacitor are due to the nanoscale radii and the nanoscale spacing of the CNTs. These nanoscale geometries make the contributions from the spill and the DOS prominent in the capacitance. Rich structures in the bias dependence of the capacitance $C(\mu)$, which originate from the Van Hove singularities peculiar to quasi-one-dimensional systems, are highlighted with the help of these conditions.

V. CONCLUSION

In conclusion, we have investigated the capacitance of the DWCNT (4,0)@(24,0) as a nanoscale coaxial-cylindrical capacitor. We have performed first-principles electronic-structure calculations based on the DFT with the LDA to obtain the responses of the capacitor to the bias application. We have found two principal quantum effects in the calculated capacitance.

First, we have found that the capacitance exhibits large and characteristic bias dependence, which reflects the DOS of the quasi-one-dimensional CNT electrodes. This is the first time that detailed analyses of such a nonlinear response of the capacitor to the bias application have been performed in CNT-based systems. Second, we have found that the calculated capacitance value is larger than what is estimated from the classical electromagnetism with the tube-wall radii. This enhancement is explained by that of the electrostatic component of the capacitance due to the quantum-mechanical spill of the stored electron density from the tube walls. We have also pointed out that these two quantum ef-

fects in the capacitance are peculiar to nanoscale systems and are highlighted by the small radii and spacing of the CNT electrodes in the present DWCNT capacitor.

The spill length of the accumulated charge and, thus, the electrostatic capacitance are *not* explained by the LU/HO states directly involved in the electron/hole accommodations under the bias-voltage application: The spill length is closely related to the bias-induced deformations, i.e., dielectric polarization, of all the occupied electron states. We have also found that the spill length in the inner CNT is almost the same as that in the outer CNT. However, the former more strongly contributes to the enhancement of the electrostatic capacitance than the latter. This is due to the higher concentration of the electric flux on the surface of the inner CNT than that on the outer CNT, reflecting the coaxial-cylindrical geometry of the present DWCNT capacitor.

The two quantum effects in the capacitance which we have found in the present paper can be utilized for design and control of CNT devices. Discontinuous increase (or decrease) in the capacitance brought about by the bias sweeping can be used to obtain highly sensitized on/off switching in CNT-based FETs or to fabricate nanoscale detectors for external molecules which are physisorbed or chemisorbed on the CNTs through electric-dipole moments or electron transfer between the molecules and the CNTs.

ACKNOWLEDGMENTS

We thank T. Endoh, K. Natori, Y. Fujimoto, J.-I. Iwata, and K. Kamiya for their stimulating discussions throughout this study. The present work is partly supported by a grant-in-aid from the Ministry of Education, Culture, Sports, Science and Technology under Contract Nos. 17064002 and 18063003. Computations were done at the Academic Computing and Communications Center, University of Tsukuba, at the Institute for Solid State Physics, University of Tokyo, and at the Research Center for Computational Science, Okazaki National Institute.

-
- ¹D. Hisamoto, T. Koga, and E. Takeda, *IEEE Trans. Electron Devices* **38**, 1419 (1991); for recent developments, see, e.g., IEDM 2007 (unpublished) (<http://www.his.com/~iedm/>).
- ²M. Masuoka, T. Endoh, and H. Sakuraba, presented at the 2002 Forth IEEE International Caracas Conference on Devices, Circuits and Systems, Aruba, 17–19 April 2002 (unpublished), pp. C015-1–C015-5.
- ³B. W. Smith, M. Monthieux, and D. E. Luzzi, *Nature (London)* **396**, 323 (1998).
- ⁴J. Solan *et al.*, *Chem. Phys. Lett.* **316**, 191 (2000).
- ⁵S. Iijima, *Nature (London)* **354**, 56 (1991).
- ⁶N. Hamada, S. I. Sawada, and A. Oshiyama, *Phys. Rev. Lett.* **68**, 1579 (1992).
- ⁷R. Saito, M. Fujita, G. Dresselhaus, and M. D. Dresselhaus, *Appl. Phys. Lett.* **60**, 2204 (1992).
- ⁸J. W. G. Wildöer, L. C. Venema, A. G. Rinzler, R. E. Smalley, and C. Dekker, *Nature (London)* **391**, 59 (1998).
- ⁹T. W. Odom, J.-L. Huang, P. Kim, and C. M. Lieber, *Nature (London)* **391**, 62 (1998).
- ¹⁰M. Fujita, K. Wakabayashi, K. Nakada, and K. Kusakabe, *J. Phys. Soc. Jpn.* **65**, 1920 (1996).
- ¹¹K. Nakada, M. Fujita, G. Dresselhaus, and M. S. Dresselhaus, *Phys. Rev. B* **54**, 17954 (1996).
- ¹²Y. Miyamoto, K. Nakada, and M. Fujita, *Phys. Rev. B* **59**, 9858 (1999).
- ¹³S. Okada and A. Oshiyama, *J. Phys. Soc. Jpn.* **72**, 1510 (2003).
- ¹⁴S. Okada and A. Oshiyama, *Phys. Rev. Lett.* **87**, 146803 (2001).
- ¹⁵S. Okada, K. Nakada, and T. Kawai, *Appl. Phys. Lett.* **90**, 103120 (2007).
- ¹⁶P. Hohemberg and W. Kohn, *Phys. Rev.* **136**, B864 (1964).
- ¹⁷W. Kohn and L. J. Sham, *Phys. Rev.* **140**, A1133 (1965).
- ¹⁸Z. Chen, J. Appenzeller, Y.-M. Lin, J. Sippel-Oakley, A. G. Rinzler, J. Tang, S. J. Wind, P. M. Solomon, and Ph. Avouris, *Science* **311**, 1735 (2006), and references therein.

- ¹⁹D. M. Ceperley and B. J. Alder, Phys. Rev. Lett. **45**, 566 (1980).
- ²⁰J. P. Perdew and A. Zunger, Phys. Rev. B **23**, 5048 (1981).
- ²¹L. -M. Peng, Z. L. Zhang, Z. Q. Xue, Q. D. Wu, Z. N. Gu, and D. G. Pettifor, Phys. Rev. Lett. **85**, 3249 (2000).
- ²²M. R. Mohammadzadeh, Physica E (Amsterdam) **31**, 31 (2006).
- ²³S. Okada and A. Oshiyama, Phys. Rev. Lett. **91**, 216801 (2003).
- ²⁴P. G. Collins, M. S. Arnold, and Ph. Avouris, Science **292**, 706 (2001).
- ²⁵N. Troullier and J. L. Martins, Phys. Rev. B **43**, 1993 (1991).
- ²⁶D. Vanderbilt, Phys. Rev. B **41**, R7892 (1990).
- ²⁷K. Uchida, H. Kageshima, and H. Inokawa, e-J. Surf. Sci. Nanotechnol. **3**, 453 (2005).
- ²⁸K. Uchida, H. Kageshima, and H. Inokawa, Phys. Rev. B **74**, 035408 (2006).
- ²⁹K. Uchida, S. Okada, K. Shiraishi, and A. Oshiyama, J. Phys. Condens. Matter **19**, 365218 (2007).
- ³⁰This is a quantum-theoretical extension of the classical procedure minimizing the energy $\Omega(Q)=Q^2/(2C)-\mu Q$ with respect to Q , which leads to the optimal quantity of the stored charge $Q(=C\mu)$ under the bias voltage μ .
- ³¹Linear combinations of inner- and outer-tube states can appear in real computations. By using unitary transformations among them, we are able to decompose them into inner-tube states and outer-tube states. The electron density is invariant irrespective of these transformations.
- ³²Tokyo *ab initio* program package (TAPP) is developed by a consortium initiated at the University of Tokyo: J. Yamauchi, M. Tsukada, S. Watanabe, and O. Sugino, Phys. Rev. B **54**, 5586 (1996); H. Kageshima and K. Shiraishi, *ibid.* **56**, 14985 (1997); O. Sugino and A. Oshiyama, Phys. Rev. Lett. **68**, 1858 (1992).
- ³³P. Pomorski, C. Roland, H. Guo, and J. Wang, Phys. Rev. B **67**, 161404(R) (2003).
- ³⁴M. Tanaka, Y. Gohda, S. Furuya, and S. Watanabe, Jpn. J. Appl. Phys., Part 2 **42**, L766 (2003).
- ³⁵M. Büttiker, J. Phys.: Condens. Matter **5**, 9361 (1993).
- ³⁶S. Tarucha, in *Mesoscopic Physics and Electronics*, edited by T. Ando *et al.* (Springer-Verlag, Heidelberg, 1998).
- ³⁷M. Kruger, M. R. Buitelaar, T. Nussbaumer, C. Schonenberger, and L. Forro, Appl. Phys. Lett. **78**, 1291 (2001).
- ³⁸H. Shimotani, T. Kanbara, Y. Iwasa, K. Tsukagoshi, Y. Aoyagi, and H. Kataura, Appl. Phys. Lett. **88**, 073104 (2006).
- ³⁹K. Uchida *et al.* (unpublished).
- ⁴⁰K. Uchida, S. Tsuneyuki, and T. Schimizu, Phys. Rev. B **68**, 174107 (2003).
- ⁴¹K. Uchida, H. Kageshima, and H. Inokawa, Jpn. J. Appl. Phys., Part 1 **44**, 8759 (2005).
- ⁴²M. Takesada, T. Yagi, M. Itoh, and S. Koshihara, J. Phys. Soc. Jpn. **72**, 37 (2003).
- ⁴³T. Hasegawa, S. Mouri, Y. Yamada, and K. Tanaka, J. Phys. Soc. Jpn. **72**, 41 (2003).
- ⁴⁴Y. Miyamoto, A. Rubio, X. Blase, M. L. Cohen, and S. G. Louie, Phys. Rev. Lett. **74**, 2993 (1995).
- ⁴⁵S. Okada, A. Oshiyama, and S. Saito, Phys. Rev. B **62**, 7634 (2000).